

## Magnon transport in noncollinear spin textures: Anisotropies and topological magnon Hall effects

Alexander Mook,<sup>1</sup> B3rge G3bel,<sup>1,2</sup> J3rgen Henk,<sup>2</sup> and Ingrid Mertig<sup>1,2</sup>

<sup>1</sup>Max-Planck-Institut f3r Mikrostrukturphysik, D-06120 Halle (Saale), Germany

<sup>2</sup>Institut f3r Physik, Martin-Luther-Universit3t Halle-Wittenberg, D-06099 Halle (Saale), Germany

(Received 7 September 2016; published 3 January 2017)

We analyze signatures of noncollinear spin textures in the magnon transport of both spin and heat by means of atomistic spin dynamics. The influence of the spin texture is demonstrated for a spin spiral and for a skyrmion lattice on a frustrated antiferromagnet. Spin spirals show an anisotropy in the longitudinal transport, whereas skyrmion lattices exhibit transverse transport, which is interpreted in terms of topology and establishes skyrmion-induced versions of magnon Hall effects. The conductivities depend sensitively on the spiral pitch and on the skyrmion size; we predict magnon Hall angles as large as 60%.

DOI: 10.1103/PhysRevB.95.020401

*Introduction.* Skyrmions are particle-like magnetic textures with nontrivial winding [1,2]; they are frequently featured in today's condensed matter research because they produce a topological contribution to the Hall effect of electrons [3] or magnons [4–8]. In the case of magnons, a transverse thermal current  $\mathbf{J}_{\text{th}}$  is predicted upon application of a temperature gradient  $\nabla T$  to a skyrmion crystal (SkX) phase [4,5]. This “topological magnon Hall effect” (TMHE) or “topological magnon Righi-Leduc effect” is solely due to the topological charge

$$w = \frac{1}{4\pi} \int \mathbf{n}(\mathbf{r}) \cdot [\partial_x \mathbf{n}(\mathbf{r}) \times \partial_y \mathbf{n}(\mathbf{r})] d^2r \quad (1)$$

of the magnetic texture  $\mathbf{n}(\mathbf{r})$ . The TMHE has three relatives since magnons do not only carry heat but also spin: the “topological magnon spin Nernst effect” (TMSNE) comprises a transverse spin current  $\mathbf{J}_s$  due to an applied temperature gradient; its Onsager reciprocal is the “topological magnon spin Ettingshausen effect” (TMSEE). If the spin current is generated by a magnetic field gradient  $\nabla B$  [9] the term “topological magnon spin Hall effect” (TMSHE) applies. Combined, they form the family of topological magnon Hall effects (Table I). The “topological” effects originate from the self-generated magnetic texture rather than from spin-orbit interactions which explicitly enter the Hamiltonian (this is the case for the “nontopological” magnon Hall effects on, for example, the ferromagnetic kagome or pyrochlore lattices [10–13]).

Linear response theory captures these effects by coupling the gradients (forces) to the current densities,

$$\begin{pmatrix} \mathbf{J}_s \\ \mathbf{J}_{\text{th}} \end{pmatrix} = \begin{pmatrix} L_{s,s} & L_{s,\text{th}} \\ L_{\text{th},s} & L_{\text{th},\text{th}} \end{pmatrix} \begin{pmatrix} \nabla B \\ -\nabla T/T \end{pmatrix}. \quad (2)$$

The generalized transport coefficients, i.e., the tensors  $L_{m,n}$  ( $m, n = s, \text{th}$ ), define the spin conductivity  $\sigma \equiv L_{s,s}$ , the magnetothermal conductivity  $\xi \equiv T^{-1} L_{s,\text{th}}$ , and the thermal conductivity  $\kappa \equiv T^{-1} (L_{\text{th},\text{th}} - L_{s,\text{th}} L_{s,s}^{-1} L_{\text{th},s})$  at temperature  $T$ . For a two-dimensional (2D) sample, the conductivities are  $2 \times 2$  tensors. The TMHE, TMSNE, and TMSHE are quantified by  $\sigma_{xy}$ ,  $\xi_{xy}$ , and  $\kappa_{xy}$ , respectively.

In this Rapid Communication, we identify signatures of noncollinear spin textures in the magnon transport by means of atomistic spin dynamics, focusing on spin spirals (Sp<sup>2</sup>)

and skyrmion lattices. The conductivities are evaluated as time integrals of current correlation functions (CCFs) in the Kubo formula [14]. We generalize the approach reported in Refs. [15,16] to a 2D frustrated magnet on a triangular lattice which exhibits a Sp<sup>2</sup> ground state; it features a helicity-degenerate SkX phase stabilized by an external magnetic field and by thermal fluctuations.

The longitudinal conductivities in the Sp<sup>2</sup> phase reveal a strong anisotropy due to the broken rotational symmetry of the lattice. Furthermore, the transverse conductivities in the SkX phase are finite, which proves the existence of the topological Hall effects of magnons. Both phenomena are studied in dependence on the strength of an external magnetic field and on the spiral pitch which mediates between the collinear ferromagnetic and an antiferromagnetic phase; magnon Hall angles as large as 60% are predicted. Our results call for experimental verification.

*Theoretical aspects.* We focus on noncollinear magnetic textures induced by frustrations and described within a 2D classical Heisenberg model. Its Hamiltonian

$$H = \sum_i h_i, \quad h_i = -B n_i^z - \frac{1}{2} \sum_{j \in N(i)} J_{ij} \mathbf{n}_i \cdot \mathbf{n}_j, \quad (3)$$

includes the isotropic symmetric exchange ( $J_{ij}$ ) and the Zeeman energy due to a magnetic field  $\mathbf{B} = B \hat{\mathbf{z}}$  applied orthogonal to the lattice (in the  $xy$  plane).  $N(i)$  is the set of all interacting neighbors of spin  $\mathbf{n}_i$  ( $\mathbf{n}_i$  unit vector at position  $\mathbf{r}_i$ ). The conservation of both the  $z$  component of the total spin and the energy allows us to formulate corresponding continuity equations and currents [17]: the total spin current  $\mathbf{J}_s \equiv \sum_i \mathbf{r}_i \partial \mathbf{n}_i^z / \partial t$  and the total thermal current  $\mathbf{J}_{\text{th}} \equiv \sum_i \mathbf{r}_i \partial h_i / \partial t$ . Using  $\dot{\mathbf{n}}_i = -\gamma \mathbf{n}_i \times \partial H / \partial \mathbf{n}_i$  ( $\gamma$  gyromagnetic ratio) with  $\partial H / \partial \mathbf{n}_i = -B \hat{\mathbf{z}} - \sum_{j \in N(i)} J_{ij} \mathbf{n}_j$ , these currents read

$$\mathbf{J}_s = \gamma \sum_{i < j} J_{ij} \mathbf{r}_{ij} \hat{\mathbf{z}} \cdot (\mathbf{n}_i \times \mathbf{n}_j), \quad (4)$$

$$\begin{aligned} \mathbf{J}_{\text{th}} = & -B \mathbf{J}_s - \gamma \sum_{\Delta_{ijk}} \frac{\chi_{ijk}}{2} [J_{ij} J_{jk} \mathbf{r}_{ik} + J_{jk} J_{ki} \mathbf{r}_{ji} \\ & + J_{ki} J_{ij} \mathbf{r}_{kj}] \end{aligned} \quad (5)$$

with the spin chirality  $\chi_{ijk} \equiv \mathbf{n}_i \cdot (\mathbf{n}_j \times \mathbf{n}_k)$  and  $\mathbf{r}_{ij} \equiv \mathbf{r}_i - \mathbf{r}_j$ . The summation  $\sum_{i < j}$  ( $\sum_{\Delta_{ijk}}$ ) is over each pair (triple) of spins

TABLE I. Family of topological magnon Hall effects. For the nomenclature, see the text.

force	transverse response	
	spin current	heat current
$\nabla B$	TMSHE	TMSEE
$\nabla T$	TMSNE	TMHE

without double counting. The term  $-B\mathbf{J}_s$  of  $\mathbf{J}_{th}$  describes the coupling of the spin current to the magnetic field; it gives rise to the magnetothermal conductivity, i.e., the magnetic analog of the thermopower.

In Ref. [18], the Hamiltonian (3) was applied to frustrated spins on a triangular lattice, brought about by positive nearest ( $J_1 > 0$ ) and negative third-nearest neighbor couplings ( $J_3 < 0$ ). As long as  $-4 < J_1/J_3 < 0$ , the ground state is a spin spiral with ordering vector  $|\mathbf{q}| = 2 \arccos[(1 + \sqrt{1 - 2J_1/J_3})/4]$  (lattice constant set to unity) along any of the three third-nearest neighbor directions. The magnetic phase diagram (spanned by  $T$  and  $B$ ) contains besides this single- $q$  ( $Sp^2$ ) phase coherent superpositions of two (double- $q$ ) and three (SkX, triple- $q$ ) spin spirals. Since Dzyaloshinskii-Moriya interaction (DMI) [19,20] is absent, the spin texture lacks a fixed handedness; in particular, the SkX phase is both helicity- and vorticity-degenerate; i.e.,  $w = 1$  and  $w = -1$  are equally likely. Yet, once a spin configuration is randomly chosen, an energy barrier separates the topologically opposite configurations.

Transport properties are studied by means of the classical Kubo formula of linear response theory [14],

$$L_{m,n}^{\mu\nu} = \int_0^\infty \frac{1}{Ak_B T} [C_{m,n}^{\mu\nu}(t) - \langle J_m^\mu(\infty) J_n^\nu(0) \rangle] dt; \quad (6)$$

$m, n = s, th$ , and  $\mu, \nu = x, y$ ;  $A$  and  $k_B$  are the sample's area and the Boltzmann constant, respectively.  $\langle J_m^\mu(\infty) J_n^\nu(0) \rangle$  has to be subtracted from the CCF  $C_{m,n}^{\mu\nu}(t) = \langle J_m^\mu(t) J_n^\nu(0) \rangle$  to account for those CCFs that do not drop to zero because of a persistent contribution caused by noncollinear magnetic textures [21,22]. For example, a  $Sp^2$  would yield a finite  $\mathbf{J}_s$  even without thermal excitations [cf. Eq. (4)].

After thermalizing (annealing) a spin cluster by Monte Carlo simulations, the ensemble average  $\langle \cdot \rangle$  in Eq. (6) is evaluated as a time average. The time evolution obeys the stochastic Landau-Lifshitz-Gilbert equation [23]

$$(1 + \alpha^2) d\mathbf{n}_i = -(1 + \alpha \mathbf{n}_i \times) [\mathbf{n}_i \times (\mathbf{B}_i d\tau + D d\mathbf{W}_i)]. \quad (7)$$

The precession of each moment about its effective field  $\mathbf{B}_i = -\partial H / \partial \mathbf{n}_i$  is damped. The Gilbert damping  $\alpha$  is in general a nonlocal and symmetric  $3 \times 3$  tensor but assumed here as a scalar. This approximation disregards the anisotropy of the damping due to the noncollinearity of the magnetic texture [24,25], and, thus, becomes better the smaller  $|\mathbf{q}|$ . As domain wall velocities decrease by texture-induced damping [26], the present method presumably overestimates the conductivities; hence, we address mainly Hall angles rather than conductivities.

Temperature is included by an additional white-noise field  $\mathbf{b}_i$  with  $D d\mathbf{W}_i = \mathbf{b}_i d\tau$ , where  $\mathbf{W}_i$  is an isotropic vector

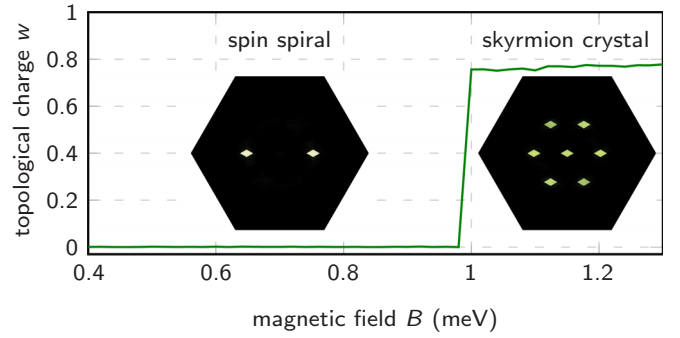


FIG. 1. Topological charge  $w$  per skyrmion for  $\lambda = 4$  versus external magnetic field  $B$ . A topological phase transition from the  $Sp^2$  phase to the SkX phase takes place at  $B \approx 1$  meV. Insets show the respective static structure factor in the structural Brillouin zone.  $J_1 = 1.171572875$  meV,  $J_3 = -1$  meV,  $T = 3$  K, and  $N \times N = 1600$ .

Wiener process and  $D^2 = 2\alpha k_B T / (2\mu_B B^{\text{ref}})$  a dimensionless diffusion constant ( $\mu_B$  Bohr's magneton).  $B^{\text{ref}}$  is a reference field determining the scale of dimensionless time  $\tau$ . For the numerical integration an implicit midpoint method is used.

The spin cluster is evolved according to Eq. (7); the currents  $\mathbf{J}_s$  and  $\mathbf{J}_{th}$  are evaluated and stored at each time step. Subsequently, the correlation functions and, finally, the transport tensors are calculated. The numerical computations showed that a total integration time of 20 ns up to 64 ns, used for all results presented below, is sufficient to converge the correlation functions.

**Results and discussion.** This Rapid Communication focuses on differences between the  $Sp^2$  and the SkX phases. Relying on finite clusters, the magnetic texture has to be commensurate: the ratio  $J_1/J_3$  is chosen such that the skyrmion lattice fits exactly. For a pitch  $\lambda = 2\pi/|\mathbf{q}|$  of the  $Sp^2$ ,  $3N^2/(4\lambda^2)$  skyrmions fit into an  $N \times N$  triangular lattice. The skyrmion lattice vectors are rotated by  $\pi/6$  with respect to the structural lattice vectors and are larger by a factor of  $2\lambda/\sqrt{3}$ .

Since the  $Sp^2$  is the ground state and the SkX phase requires elevated temperatures and a finite magnetic field  $B$ , the magnetic phase diagram is traversed by varying  $B$  at a given  $T$  (Fig. 1). For  $\lambda = 4$ , the SkX phase is formed for  $B \geq 1$  meV; larger skyrmions would require smaller critical fields. Due to thermal fluctuations and the quite small size of the skyrmions, the computed topological charge  $w$  is underestimated ( $\approx 0.8$  instead of 1). The static structure factor  $\langle \mathbf{n}^*(\mathbf{k}) \cdot \mathbf{n}(\mathbf{k}) \rangle$  [ $\mathbf{n}(\mathbf{k})$  lattice Fourier transform of the magnetic texture] retrieves the ordering vectors: a single pair of ordering vectors (two spots) for the  $Sp^2$  phase and three pairs (six spots) in the SkX phase (the central, seventh spot belongs to the ferromagnetic contribution). A further increase of  $B$  leads to the double- $q$  phase and, finally, to the field-polarized phase [18] (not shown).

Concerning transport, we focus on the thermal CCF and note that the following discussion is qualitatively valid for the other CCFs, too. The  $Sp^2$  breaks the sixfold structural rotational symmetry about the  $z$  axis. We consider samples with  $\mathbf{q}$  along the  $x$  axis to facilitate the discussion. This broken symmetry yields  $C_{th,th}^{xx} \neq C_{th,th}^{yy}$  [red and blue curves as well as vertical arrow in Fig. 2(a)]. Since  $C_{th,th}^{xy} = C_{th,th}^{yx} = 0$

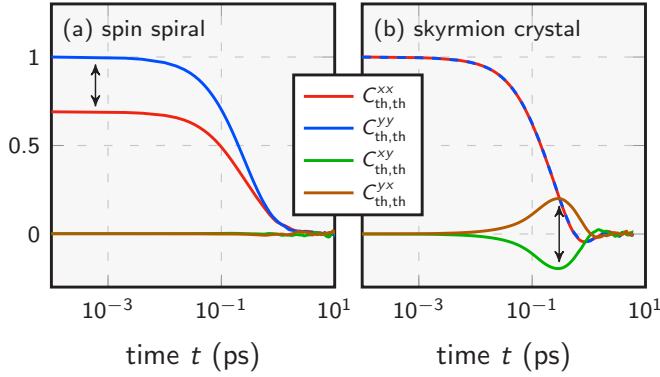


FIG. 2. Time dependence of the longitudinal (blue:  $C_{th,th}^{xx}$ , red:  $C_{th,th}^{yy}$ ) and transverse (green:  $C_{th,th}^{xy}$ , brown:  $C_{th,th}^{yx}$ ) thermal current correlation functions in the  $Sp^2$  (a) and in the SkX phase (b). The CCFs are normalized to their value at  $t = 0$ . Vertical arrows indicate signatures unique to the respective magnetic phase. Parameters as in Fig. 1 with  $B = 0.6$  meV and  $B = 1.2$  meV in the  $Sp^2$  and SkX phase, respectively.

(green and brown curves) there is no transverse transport [27]. Furthermore, the longitudinal spin correlation function along  $\mathbf{q}$  does not drop to zero (not shown) since the  $Sp^2$  introduces a persistent contribution to the microscopic currents which is removed to determine the true transport [Eq. (6)].

The SkX phase maintains  $C_{th,th}^{xx} = C_{th,th}^{yy}$  because the rotational symmetry of the triangular lattice is not broken [Fig. 2(b)]. Most notably, the off-diagonal part of the transport tensor is antisymmetric and nonzero [ $C_{th,th}^{xy} = -C_{th,th}^{yx} \neq 0$ ; green and brown curves as well as vertical arrow in Fig. 2(b)] which indicates transverse transport.

The above signatures due to the magnetic textures— $C_{th,th}^{xx} \neq C_{th,th}^{yy}$  and  $C_{th,th}^{xy} = C_{th,th}^{yx} = 0$  for the  $Sp^2$  but  $C_{th,th}^{xx} = C_{th,th}^{yy}$  and  $C_{th,th}^{xy} = -C_{th,th}^{yx} \neq 0$  for the SkX—show up also in the dependence of the conductivities on the external magnetic field (Fig. 3).  $\sigma_{\mu\mu}$  and  $\kappa_{\mu\mu}$  [red and blue symbols, respectively, in Figs. 3(a) and 3(c)] are positive.  $\xi_{\mu\mu}$  being negative (b) implies that the transport is dominated by spin-down particles (relative to  $\mathbf{B}$ ), which is readily understood by the magnons having largely spin antiparallel to the net magnetization which itself is along  $\mathbf{B}$ .

In the  $Sp^2$  phase ( $B \lesssim 1$  meV),  $\sigma_{xx} > \sigma_{yy}$  [red and blue symbols, respectively, and vertical arrow in (a)] translates to  $|\xi_{xx}| < |\xi_{yy}|$  [see (b)] since  $\xi = T^{-1}\sigma^{-1}L_{s,th}$ . This relation, although less prominent, is “transferred” to  $\kappa_{xx} < \kappa_{yy}$  [see (c)]. Thus, we conclude that thermal and spin transport are differently influenced: thermal transport along the ordering vector  $\mathbf{q}$  is less efficient than perpendicular to it, whereas the opposite holds for spin transport.

This anisotropy is lost (red and blue curves coincide) once the SkX phase is reached ( $B \gtrsim 1$  meV). The transverse conductivities (green and brown symbols in Fig. 3), which are approximately zero within the  $Sp^2$  phase, take on small but nonzero values. They are antisymmetric; that is, an  $xy$  and a  $yx$  element differ in sign but not in modulus. Thus, all of the transverse transport phenomena mentioned above are present.

Longitudinal transport does not depend on whether a skyrmion ( $w > 0$ ) or an antiskyrmion lattice ( $w < 0$ ) is formed

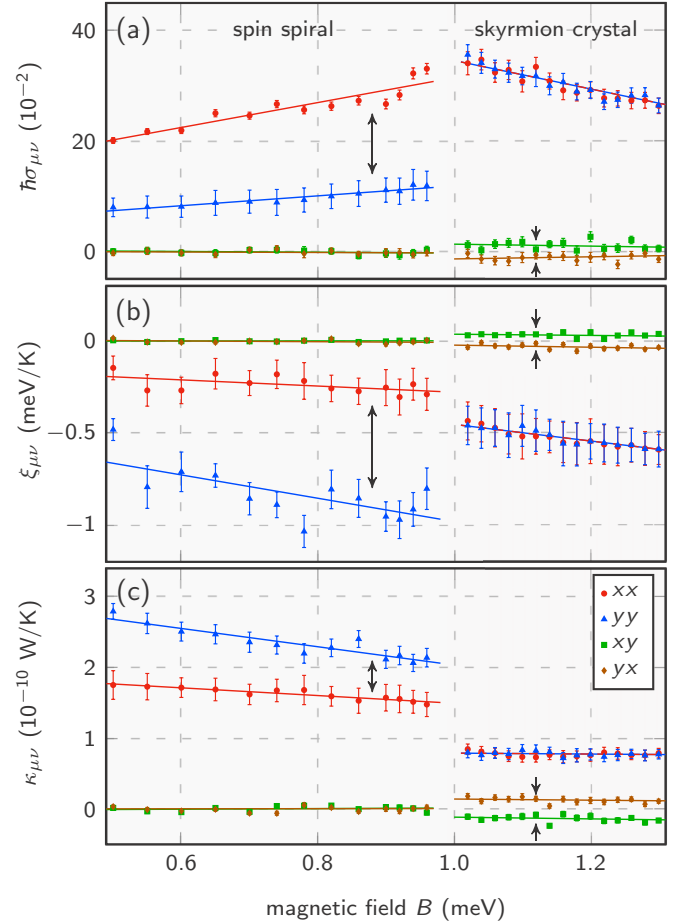


FIG. 3. Spin conductivity  $\sigma_{\mu\nu}$  (a), magnetothermal conductivity  $\xi_{\mu\nu}$  (b), and thermal conductivity  $\kappa_{\mu\nu}$  (c) versus external magnetic field for  $\lambda = 4$  ( $\mu, \nu = x, y$ ). Parameters as in Fig. 1, Gilbert damping  $\alpha = 0.05$ ,  $\sigma$  multiplied by  $\hbar$ . Lines are guides to the eye; vertical arrows indicate signatures unique to the respective magnetic phase.

during annealing. However, the sign of  $w$  determines the sign of the transverse CCFs and of the transverse conductivities. This feature is explained by the “emergent electrodynamics” of magnons, originally derived for electrons [3]. A local coordinate transformation to the reference frame of the skyrmion texture recasts Eq. (7) to look formally like an equation describing charged particles in (fictitious) electromagnetic fields [4,5,28,29]. In particular, an emergent magnetic field  $B_{em}$  along the  $z$  direction is identified, which contains the local contribution to  $w$  [Eq. (1)]. Inversion of  $w$  inverts  $B_{em}$ , the emergent Lorentz force, and, consequently, the transverse transport direction.

Restricting ourselves to samples with  $w > 0$ , we discuss the effect of the pitch  $\lambda$  on both the transport anisotropy—quantified by  $\kappa^{xx}/\kappa^{yy}$ —in the  $Sp^2$  phase and on the magnon Hall transport in the SkX phase. The stabilization of large skyrmions requires different exchange parameters, temperatures, and magnetic fields. This implies that a direct comparison of transverse conductivities is barely meaningful. Therefore, we focus on the (thermal) magnon Hall angle  $\kappa_{xy}/\kappa_{xx}$  because it is accessed easily in experiments [11,30,31]; its discussion applies also to the other conductivities.

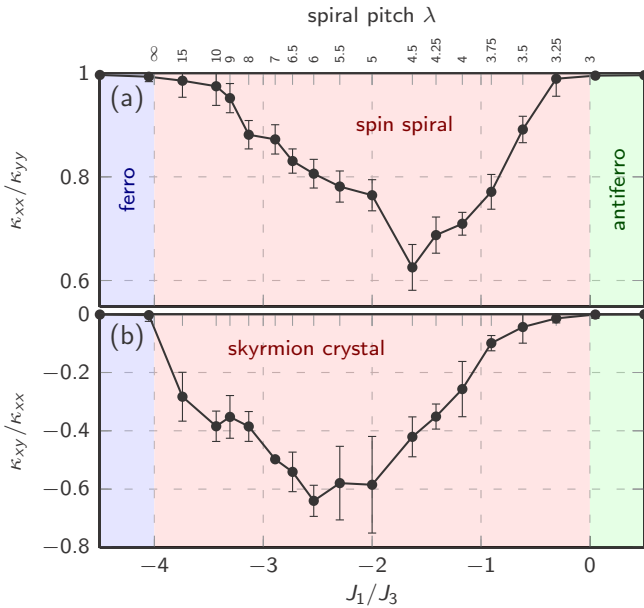


FIG. 4. (a) Longitudinal transport anisotropy  $\kappa_{xx}/\kappa_{yy}$  in the  $\text{Sp}^2$  phase. The ordering vector is along the  $x$  direction. (b) Magnon Hall angle  $\kappa_{xy}/\kappa_{xx}$  in the SkX phase versus  $J_1/J_3$  ( $J_1 > 0$ ). Three magnetic phases are indicated: collinear ferromagnetic phase (blue, “ferro”),  $\text{Sp}^2/\text{SkX}$  phase (red), and the antiferromagnetic phase (green, “antiferro”). For  $-4 < J_1/J_3 < 0$  the ratio  $J_1/J_3$  translates into the  $\text{Sp}^2$  pitch  $\lambda$  and the corresponding skyrmion size. Cluster sizes were chosen such that the magnetic textures are commensurate.  $B$  and  $T$  had to be varied for the formation of the SkX phase;  $\alpha = 0.05$ . For the  $\text{Sp}^2$  phase the magnetic field is half as large as in the SkX phase.

For the variation of the magnetic texture two limits have to be noted: (i)  $\lambda$  decreases for  $J_1/J_3 \nearrow 0$  until it is so small that the spatial frequency of the lattice sites is too small to sample the  $\text{Sp}^2$ , and an antiferromagnetic phase is formed; and (ii)  $\lambda$  increases for  $J_1/J_3 \searrow -4$  up to infinity, which generates a collinear ferromagnetic order for  $J_1/J_3 \leq -4$ .

Neither the ferromagnetic nor the antiferromagnetic phase breaks the structural symmetry of the triangular lattice; therefore,  $\kappa^{xx}/\kappa^{yy} = 1$  is found [Fig. 4(a)]. Only within the  $\text{Sp}^2$  phase ( $-4 < J_1/J_3 < 0$ ) an anisotropy of up to  $\approx 0.7$  is identified and reached at  $\lambda = 4 \sim 5$ .

While the magnon Hall angle  $\kappa_{xy}/\kappa_{xx}$  is zero in the (collinear) ferromagnetic and antiferromagnetic phases [Fig. 4(b)], it is negative in the SkX phase, showing a minimum of about  $-60\%$  at  $\lambda = 5 \sim 6.5$ . Its absolute value is much larger than in systems showing the (nontopological) MHE (ferromagnetic kagome lattice:  $\approx 10^{-2}$  [12,13,31,32]; pyrochlore lattice:  $\approx 10^{-3}$  [11,30]). The increase of  $|\kappa_{xy}/\kappa_{xx}|$  with decreasing  $\lambda$  down to  $\lambda \approx 6$  is explained by the increasing

skyrmion density (decreased skyrmion size) and the increasing density of  $B_{\text{em}}$  (the same trend is found for electrons [33]). Although the skyrmion density increases as  $J_1/J_3 \nearrow 0$  (further decrease of  $\lambda$ ), the Hall angle drops to zero, which we attribute to the quite coarse sampling underestimating  $w$  and  $B_{\text{em}}$ .

Concerning the temperature dependence of the conductivities, we recall that the spins are treated classically: spin and energy are not quantized; the Boltzmann distribution is used. This ansatz is “borrowed” from molecular dynamics simulations [34] for the evaluation of the phonon thermal conductivity; one of its drawbacks is that  $\kappa$  diverges for  $T \rightarrow 0$  [35]. *Ad hoc* “quantum corrections” restore the limit  $\kappa \rightarrow 0$  [37] and could be implemented here as well. However, care has to be taken for  $\kappa_{xy}$ ; it diverges not alone because of the classical treatment but also because a direct application of the Kubo formula yields a nonphysical divergence for  $T \rightarrow 0$ . The latter is attributed to circulating heat currents [38] which are not experimentally observable, so their contribution has to be removed. Hence, “quantum corrections” without proper removal of circulating currents appear questionable but have to be applied for models which feature a SkX phase at  $T = 0$  [39,40]; in the present case, which requires elevated temperatures, quantum corrections are not necessary. In particular, we point out that our numerical results obey Onsager’s reciprocity relation.

**Outlook.** The identified signatures of the noncollinear magnetic textures in the magnon transport of spin and heat are accessible in experiments. The magnon spin Hall effect or the magnon spin Nernst effect require measuring spin currents, using the inverse spin Hall effect [41].

To measure the transverse thermal conductivity, we suggest an electrically insulating material that exhibits a spin spiral as ground state and which features a SkX phase at an elevated external magnetic field; examples are  $\text{Cu}_2\text{OSeO}_3$  [42] and  $\text{BaFe}_{1-x-0.05}\text{Sc}_x\text{Mg}_{0.05}\text{O}_{19}$  [43], both of which show SkX phases induced by DMI rather than by frustration. Nonetheless, when traversing the phase boundary between the  $\text{Sp}^2$  and the SkX phase by increasing the magnetic field, the longitudinal transport anisotropy should abruptly vanish and transverse thermal transport should set in [Fig. 3(c)]. For small skyrmions, magnon Hall angles are expected orders of magnitudes larger than in systems showing the (nontopological) MHE [11,30,31].

It is conceivable to extend the numerical method to three dimensions and to include magnetocrystalline anisotropies. Taking into count the DMI would allow us to apply the approach to topological magnon insulators [10–13,31,32,44–52] and to DMI-induced SkX phases exhibiting an additional spin-orbit contribution to the transverse conductivities [4].

**Acknowledgments.** This work is supported by SPP 1666 of Deutsche Forschungsgemeinschaft (DFG).

[1] S. Mühlbauer, B. Binz, F. Jonietz, C. Pfleiderer, A. Rosch, A. Neubauer, R. Georgii, and P. Boni, *Science* **323**, 915 (2009).  
 [2] N. Nagaosa and Y. Tokura, *Nat. Nanotechnol.* **8**, 899 (2013).

[3] T. Schulz, R. Ritz, A. Bauer, M. Halder, M. Wagner, C. Franz, C. Pfleiderer, K. Everschor, M. Garst, and A. Rosch, *Nat. Phys.* **8**, 301 (2012).

- [4] K. A. van Hoogdalem, Y. Tserkovnyak, and D. Loss, *Phys. Rev. B* **87**, 024402 (2013).
- [5] M. Mochizuki, X. Z. Yu, S. Seki, N. Kanazawa, W. Koshibae, J. Zang, M. Mostovoy, Y. Tokura, and N. Nagaosa, *Nat. Mater.* **13**, 241 (2014).
- [6] C. Schütte and M. Garst, *Phys. Rev. B* **90**, 094423 (2014).
- [7] Y.-T. Oh, H. Lee, J.-H. Park, and J. H. Han, *Phys. Rev. B* **91**, 104435 (2015).
- [8] S. Komineas and N. Papanicolaou, *Phys. Rev. B* **92**, 064412 (2015).
- [9] S. Fujimoto, *Phys. Rev. Lett.* **103**, 047203 (2009).
- [10] H. Katsura, N. Nagaosa, and P. A. Lee, *Phys. Rev. Lett.* **104**, 066403 (2010).
- [11] Y. Onose, T. Ideue, H. Katsura, Y. Shiomi, N. Nagaosa, and Y. Tokura, *Science* **329**, 297 (2010).
- [12] A. Mook, J. Henk, and I. Mertig, *Phys. Rev. B* **89**, 134409 (2014).
- [13] H. Lee, J. H. Han, and P. A. Lee, *Phys. Rev. B* **91**, 125413 (2015).
- [14] R. Kubo, M. Toda, and N. Hashitsume, *Statistical Physics II* (Springer, Berlin, 1991).
- [15] A. V. Savin, G. P. Tsironis, and X. Zotos, *Phys. Rev. B* **72**, 140402 (2005).
- [16] B. Jenčič and P. Prelovšek, *Phys. Rev. B* **92**, 134305 (2015).
- [17] G. D. Mahan, *Many-Particle Physics* (Springer Science+Business Media, 2000).
- [18] T. Okubo, S. Chung, and H. Kawamura, *Phys. Rev. Lett.* **108**, 017206 (2012).
- [19] I. Dzyaloshinsky, *J. Phys. Chem. Solids* **4**, 241 (1958).
- [20] T. Moriya, *Phys. Rev.* **120**, 91 (1960).
- [21] F. Schuetz, P. Kopietz, and M. Kollar, *Eur. Phys. J. B* **41**, 557 (2004).
- [22] G. Tatara, *Phys. Rev. B* **92**, 064405 (2015).
- [23] B. Skubic, J. Hellsvik, L. Nordström, and O. Eriksson, *J. Phys.: Condens. Matter* **20**, 315203 (2008).
- [24] Z. Yuan, K. M. D. Hals, Y. Liu, A. A. Starikov, A. Brataas, and P. J. Kelly, *Phys. Rev. Lett.* **113**, 266603 (2014).
- [25] C. A. Akosa, I. M. Miron, G. Gaudin, and A. Manchon, *Phys. Rev. B* **93**, 214429 (2016).
- [26] J. Foros, A. Brataas, Y. Tserkovnyak, and G. E. W. Bauer, *Phys. Rev. B* **78**, 140402 (2008).
- [27]  $C_{th,th}^{xy} = C_{th,th}^{yx} \neq 0$  if  $\mathbf{q}$  were not aligned with one of the Cartesian axes; a principal-axis transformation would then be necessary.
- [28] A. A. Kovalev, *Phys. Rev. B* **89**, 241101 (2014).
- [29] U. Güngördü and A. A. Kovalev, *Phys. Rev. B* **94**, 020405 (2016).
- [30] T. Ideue, Y. Onose, H. Katsura, Y. Shiomi, S. Ishiwata, N. Nagaosa, and Y. Tokura, *Phys. Rev. B* **85**, 134411 (2012).
- [31] M. Hirschberger, R. Chisnell, Y. S. Lee, and N. P. Ong, *Phys. Rev. Lett.* **115**, 106603 (2015).
- [32] R. Chisnell, J. S. Helton, D. E. Freedman, D. K. Singh, R. I. Bewley, D. G. Nocera, and Y. S. Lee, *Phys. Rev. Lett.* **115**, 147201 (2015).
- [33] N. Nagaosa, J. Sinova, S. Onoda, A. H. MacDonald, and N. P. Ong, *Rev. Mod. Phys.* **82**, 1539 (2010).
- [34] D. Rapaport, *The Art of Molecular Dynamics Simulation* (Cambridge University Press, Cambridge, UK, 2004).
- [35] For magnons, this divergence is only found for a perfect crystal for  $\alpha = 0$  [15]. For  $\alpha > 0$ ,  $\kappa \rightarrow \text{const.}$ , and disorder yields  $\kappa \rightarrow 0$  [16]. The latter recovers the Wiedemann-Franz law of magnon transport [36].
- [36] K. Nakata, P. Simon, and D. Loss, *Phys. Rev. B* **92**, 134425 (2015).
- [37] J. E. Turney, A. J. H. McGaughey, and C. H. Amon, *Phys. Rev. B* **79**, 224305 (2009).
- [38] T. Qin, Q. Niu, and J. Shi, *Phys. Rev. Lett.* **107**, 236601 (2011).
- [39] A. O. Leonov and M. Mostovoy, *Nat. Commun.* **6**, 8275 (2015).
- [40] A. Roldán-Molina, A. S. Nunez, and J. Fernández-Rossier, *New J. Phys.* **18**, 045015 (2016).
- [41] E. Saitoh, M. Ueda, H. Miyajima, and G. Tatara, *Appl. Phys. Lett.* **88**, 182509 (2006).
- [42] S. Seki, X. Z. Yu, S. Ishiwata, and Y. Tokura, *Science* **336**, 198 (2012).
- [43] X. Yu, M. Mostovoy, Y. Tokunaga, W. Zhang, K. Kimoto, Y. Matsui, Y. Kaneko, N. Nagaosa, and Y. Tokura, *Proc. Natl. Acad. Sci. USA* **109**, 8856 (2012).
- [44] R. Matsumoto and S. Murakami, *Phys. Rev. Lett.* **106**, 197202 (2011).
- [45] R. Matsumoto and S. Murakami, *Phys. Rev. B* **84**, 184406 (2011).
- [46] R. Shindou, R. Matsumoto, S. Murakami, and J.-i. Ohe, *Phys. Rev. B* **87**, 174427 (2013).
- [47] L. Zhang, J. Ren, J.-S. Wang, and B. Li, *Phys. Rev. B* **87**, 144101 (2013).
- [48] A. Mook, J. Henk, and I. Mertig, *Phys. Rev. B* **90**, 024412 (2014).
- [49] E. A. Nytko, J. S. Helton, P. Müller, and D. G. Nocera, *J. Am. Chem. Soc.* **130**, 2922 (2008).
- [50] R. Cheng, S. Okamoto, and D. Xiao, *Phys. Rev. Lett.* **117**, 217202 (2016).
- [51] V. A. Zyuzin and A. A. Kovalev, *Phys. Rev. Lett.* **117**, 217203 (2016).
- [52] A. Mook, J. Henk, and I. Mertig, *Phys. Rev. B* **94**, 174444 (2016).